TECHNICAL PAPER

Design and simulation of millimeter wave reconfigurable antenna using iterative meandered RF MEMS switch for 5G mobile communications

P. Ashok Kumar[1] · K. Srinivasa Rao[1] · K. Girija Sravani[1,2]

Abstract

This paper present the design and simulation of a circular patch antennas integrated with low pull in voltage novel iterative meander RF MEMS switch. The transmitting signal can be alternatively switch from 40 to 60 GHz by actuating the switch beams placed on the feeding line of patch antenna. The switch—B is actuated to allow the RF (radio frequency) signal to pass through switch—A to radiates the signal at 40 GHz and it is vice versa for the signal is radiating at 60 GHz. This type of antenna is used for future 5G (5th generation) mobile communication applications. The switch utilizes 1.6 V of actuation voltage and 1.63 µs (micro seconds) of transition time to displace the beam from upstate to downstate. It exhibits very low return loss and insertion losses of − 56 dB (decibels) and − 0.19 dB at 40 GHz (gigahertz), respectively and shows high isolation of − 37.5 dB at 45 GHz such that efficiently used for millimeter wave applications. The two circular patch antennas are designed at 40 GHz and 60 GHz shows good performance characteristics and are alternatively switch between them when signal conjunction occurs. The characteristics of switch and antennas are studied by using FEM (finite element modeling) tools such as COMSOL, HFSS 13.0 V and CST 15.0 V and tunability of the antenna is achieved efficiently for 5G mobile applications.

1 Introduction

From the past 50 years, the wireless mobile communications have been revolutionized the way of people communicate with each other (Zalud 2002). Cellular mobiles are introduced in the end of twentieth century and the rapid development in the device architectures, high speed, large data transfer and its convenience to handle made them to evolve as an significant device in our daily life communications. The first generation (1G) mobile phones are evolved as an analog systems and are developed to the digital systems in second generation (2G). The advancement in the digital technology made these mobiles to transfer the multimedia messages which has given rise to third generation (3G) mobile phones with 2 Mbps speed. Later the evolution of 4G technology with LTE and VoLTE systems have been developed to transfer the data with high bit rate of 100 Mbps. The frequency band which is utilized for 4G technology ranges from 1 to 2.6 GHz. However, the 4G technology has been employed almost in all countries but it still cannot accommodated to some challenges such as crisis in spectrum, high consumption of energy, poor coverage, low quality of service (QoS), bad interconnection and lack of flexibility etc. (Aydemir and Cengiz 2016; Hong et al. 2014). The evolution of 5G technology will address the demands and challenges associated with the past generations and leads to the existence of smart systems in future. A new concept in design approach is require to facilitate all the needs and challenges in the 5G technology (Haraz 2015; Borah et al. 2016). The radical growth in traffic, trade-offs between the capacity requirements and shortage of spectrum urges the need of millimetre wave (mm wave) technology which ranges from 30 to 300 GHz for the 5G mobile networks (Niu et al.

✉ P. Ashok Kumar
 ashok09411@gmail.com

✉ K. Srinivasa Rao
 srinivasakarumuri@gmail.com

[1] Department of Electronics and Communication Engineering, MEMS Research Center, Koneru Lakshmaiah Education Foundation (Deemed to be University), Green Fields, Vaddeswaram, Guntur 522502, India

[2] Department of Electronics and Communication Engineering, National MEMS Design Center, National Institute of Technology, Silchar, Silchar, Assam 788010, India

2015). The 5G mobile communications utilizes the frequency below 45 GHz and 60 GHz (IEEE 802.11) for 5G mobile communication systems (Mukherjee et al. 2016). Antennas are the primary components used to transmit and receive the signals at the mobile base stations as well as mobile switching centres. Reconfigurability in its frequency is used to switch between two frequencies to overcome the traffic congestion (George et al. 2017). Frequency reconfigurable antennas can change their frequency according to the desired application functionality. The shifting between the frequencies is carried out by altering its radiating wavelength by using switching elements such as PIN diodes, FETs and RF MEMS switches. Among them RF MEMS switches are efficiently used due to their low power consumption, good RF performance characteristics and miniaturization (Brown 1998).

A novel approach to design wideband fractal antennas are (a) Minkowski patches, (b) Koch dipole (c) Log-periodic printed dipole (d) Equilateral Sierpinski gasket (e) Obtuse angle Sierpinski gasket have been designed and are integrated with RF MEMS switches for reconfigurability in their radiating frequency of the antennas (Anagnostou et al. 2001). A microstrip rectangular loop antenna integrated with DC contact RF MEMS switch is proposed and the reconfigurability in the frequency is observed by simulating the proposed antenna with switch using electromagnetic full wave analysis simulation tool. The resonant frequency of the microstrip loop antenna is shown to be reconfigurable linearly by 56% with the linear change of the physical perimeters (Zhou et al. 2007). A multistate RF MEMS switches are integrated with the antenna. Three switches were employed on the U-slotted rectangular antenna and the switch exhibits seven different states of operation.

The three switches are operating at the resonant frequency of 1.8 GHz, 4.18 GHz and 5.56 GHz, respectively (Pourziad et al. 2013). A novel switch with circular capacitive area is designed to reconfigure the frequency of the antenna. The switch suffers from high pull in voltage of 14 V (Xu et al. 2018) which is not suitable for mobile communication applications. At present many researches and companies have developed reconfigurable antenna using RF MEMS switches but still facing the challenges such as pull in voltage, trade-off between RF and electromechanical performance, slow switching time etc.

In this paper, a novel antenna with two circular patch combinations is presented and they are alternatively switched by a novel RF MEMS switch to work at 5G mobile communication system. The two circular patch antennas are designed to radiate at 40 GHz and 60 GHz frequencies, respectively and based on the signal congestion the frequency is shifted between them by actuating the desired switches. A novel iterative meander switch is mounted on the CPW feed of the antennas for fast switching with low pull in voltage. The performance of the switch at the proposed frequency is studied and the characteristics of the antennas such as return loss, radiation pattern, bandwidth, power radiation, gain and directivity has been analyzed at different switching conditions.

2 Design and operation

The cellular network system generally divided in the clusters or cells at the particular frequency bands. Each cell consists of a public telecommunication switching network, mobile switching center and base station transceivers between two mobile stations. The base station transceiver receives the signal from the transmitting mobile station and public telecommunication switching network selects the particular mobile switching network where the end user mobile station is located. The mobile switching network identifies the end-user mobile station and switches the base station nearer to it. The base station transceiver communicates with the end-user and establishes the connection between the mobiles (cell phones). Figure 1 describes the pictorial description of cellular network system and it contains the antennas at each station to establish an end—to—end connections. If the total number of users in the cell is increased there exists a signal congestion (more traffic) which leads to poor establishment of connections. Hence for 5G communication there is a need to switch between two frequencies to overcome the traffic challenges. The main object of the paper is to propose an antenna which can be able to shift from 40 to 60 GHz by using RF MEMS switches.

The proposed antenna structure consists of patch elements placed over the thick insulating layer of 2 µm thickness made up of silicon dioxide which in turn mounted on a thick silicon substrate of height 450 µm as shown in Fig. 2. The material selection of the switch and the antenna is carried out by Ashby's approach where the ranking is done by material and performance indices. The best suited materials are considered for the switch and antenna to transmit RF signal with high reliability (Sharma and Gupta 2012).

The patch over the silicon dioxide layer consists of two circular patch antennas with the centers separated by a distance of 1825 µm such that it does not influenced by the aperture coupling. Figure 3 describes the top view of the patch antenna with two circular patches fed by power divider circuit of CPW. The schematic consists of left side circular patch, designed with the radius of 800 µm which radiates at 40 GHz and the right-side patch with the radius of 525 µm used to radiate at the frequency of 60 GHz. These two patches of antenna are accommodated with the
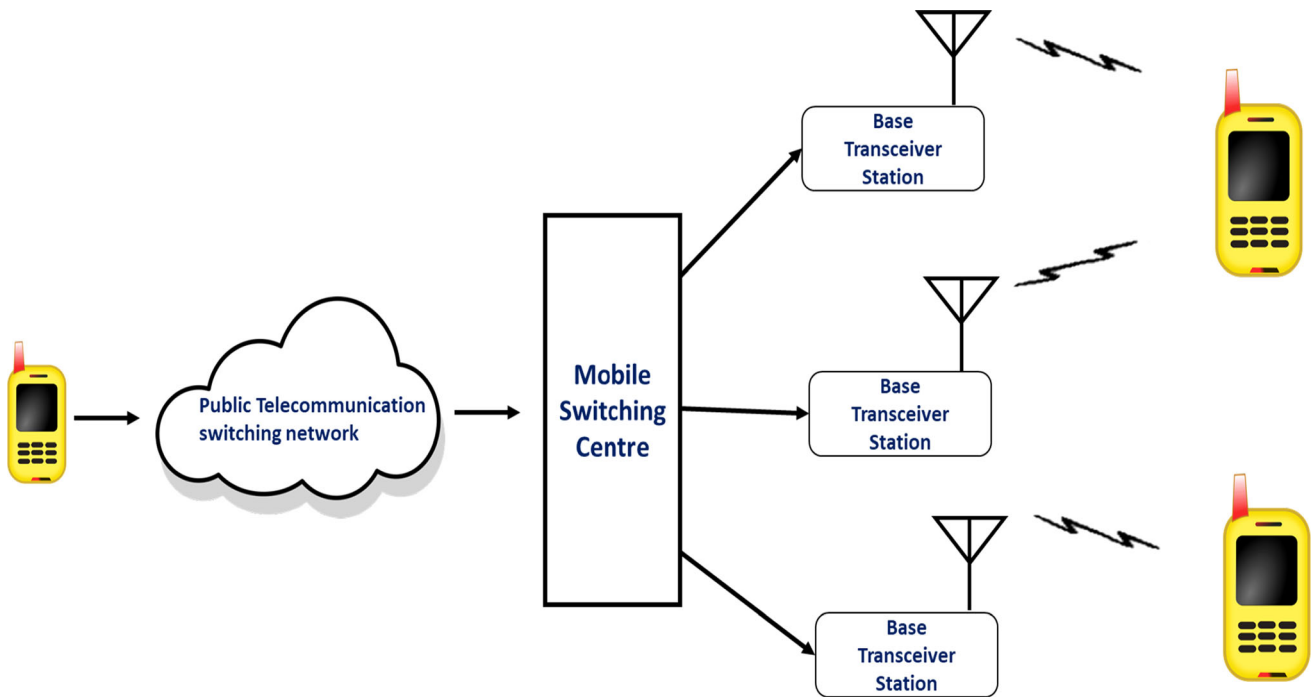
Fig. 1 The conception view of cellular network system

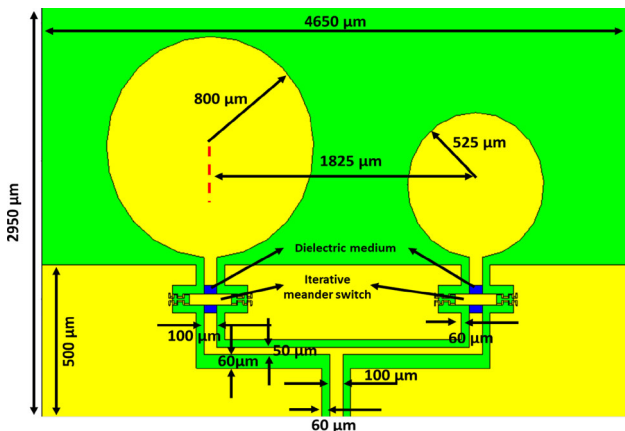Fig. 2 View of micromachining part of the antenna

Fig. 3 The dimensions of the circular patch integrated with RF MEMS switches

RF MEMS switches on their CPW feed such that these are alternatively switched according to the frequency of mobile stations during signal congestion.

The microwave power divider using CPW technology is considered as the feeding technique to couple the input RF signal to the circular patches and the portion of the power divider is presented in the Fig. 4. The T-shaped power divider is chosen as the appropriate type to design the feeding line of antenna integrated with switch. Initially, the signal line width of 100 μm with 60 μm ground plane spacing is chosen to get 50 Ω characteristics. The two arms are then extended in right and left sides to arise the power divider concept and these arms are having signal line width of 50 μm with a ground line spacing of 60 μm. The total characteristic impedance of obtained for the two arms is denoted as Z_t and is expressed as
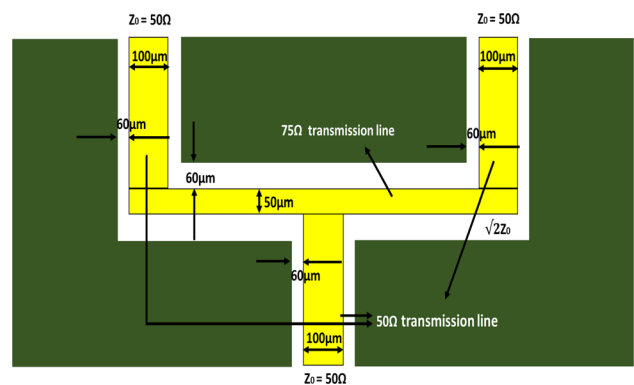
$$Z_t = \sqrt{2}Z_0 \tag{1}$$

Fig. 4 Power divider CPW feeding technique

where Z_t is the characteristic impedance of each arm and Z_0 is the characteristic impedance of initial CPW feed line. A total impedance of 75 Ω is obtained with the geometrical dimensions of the arms and these are then connected with the feed lines of antenna with initial CPW configuration which is 60/100/60 where 50 Ω characteristic impedance is achieved to transmit the signal without distortions. Hence a total power (2P) at the initial stage of feeding is then reduce to its half and the signal with power P is transmitted to the antenna to radiate.

The 5G mobile communication utilizes the higher frequency bands at 39 GHz and 60 GHz. The alternate switching between these frequencies is achieved by proposing an identical iterative meander switches taken on the feeds of antennas as shown in Fig. 5. The conductors which are connected to the arms of the power divider will serves as the signal line for the RF MEMS switches. The switch is a metallic beam suspended by using a iterative serpentine structure meanders over the signal line with an air gap of 2 μm. These meanders are anchored on the ground planes which are present on the either side of the signal line. A thin dielectric layer of thickness 0.3 μm made up of silicon nitrides is placed over the signal line to generate capacitance between suspended beam signal line. Two biasing pads are placed just below the suspending beam with air gap of 2 μm on either side of the signal line. These biasing pads are supplied with the voltage during actuation (Katehi et al. 2002). A novel type iterative meanders are used to suspend the beam provides a very low spring constant which reduces pull in voltage.

The figure of merit of device depends upon the different aspect such as return loss, radiating efficiency, directivity of the antennas and capacitance ratio, pull in voltage of the switch for which the dimensions are shown in the Table 1 (Öjefors 2004).

The proposed schematic of the switch is based on fixed—fixed type capacitive shunt configuration as shown in the Fig. 6. Initially, when no voltage is applied to the
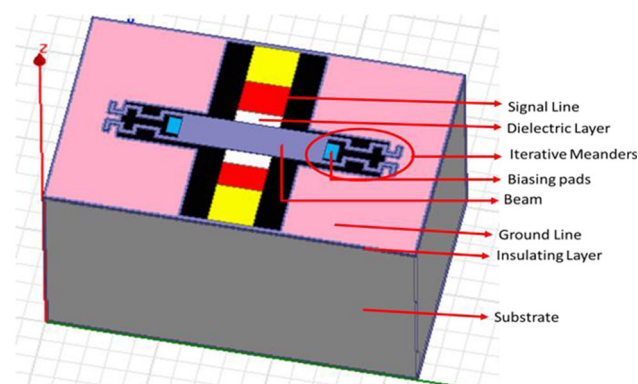
biasing pads the suspended beam will be in rest position such that an air gap of 2 μm is available between the dielectric medium and suspended beam. The RF signal is coupled between central conductor (signal line) and ground lines on either side with 1 mV for transmission of signal to output port and this results in formation of low capacitive (C_{up}) and offers low impedance to transmit the signal to output port. This capacitance is referred as upstate capacitance or on state capacitance.

When an actuation voltage is applied between the biasing pads and suspended beam connected to the ground lines. An electrostatic force is developed and pulls the suspended beam downwards. This downward movement of beam decreases the gap between dielectric layer and beam as shown in Fig. 7 and increases the capacitance between them. A large capacitance is developed between the biasing pads and beam and this is in parallel with the capacitance between beam and dielectric. The overall capacitance obtained is called downstate capacitance or off-state capacitance and it offers high impedance to RF signal to reach the output. In this condition the switch does not transmits the RF signal and remains in off-state until the actuation voltage is removed.

3 Proposed fabrication process of antenna integrated with RF MEMS switch

A thick layer of silicon wafer of having thickness 450 μm is formed as shown in Fig. 8a by wafer processing method. The proposed antenna utilizes high resistivity silicon as a substrate material to obtain low substrate losses. The surface of the substrate is then oxidized to forma a thin layer of silicon dioxide which acts as a insulator is presented in Fig. 8b. A thin layer of photo resist material is deposited and a mask is defined to form patterns of CPW and antenna regions as shown in Fig. 8c. The lithography process is carried out and the regions exposed to UV rays is etched as shown in Fig. 8d. The region defined for CPW and antenna is deposited by the gold material and the remaining photo resist material is etched to form and antenna and CPW region as shown in Fig. 8e. Here PECVD technique is followed for deposition process hence the conductors with high yield and less tolerance to the moisture occurs and helps the device to work with high lifetime. The portion of the antenna region where the switch has to be integrated is represented in the Fig. 8f as a cross sectional view. Here, the CPW lines with slots and biasing pads are define for the fabrication of switch over the antenna feeds. A thin layer of photo resist and a mask to define the dielectric layer is considered in this step and is exposed to UV rays as shown in Fig. 8g. A portion of the photoresist is etched to form a grove on it as shown in Fig. 8h to define the dielectric

Fig. 5 The schematic view of the proposed RF MEMS switch

Signal Line
Dielectric Layer
Iterative Meanders
Biasing pads
Beam
Ground Line
Insulating Layer
Substrate

Table 1 Device specifications of the proposed RF MEMS switch

S. no	Component	Length (μm)	Width (μm)	Height (μm)	Material
1	Substrate	4650	2950	450	Silicon
2	Insulating layer	4650	2950	2	SiO$_2$
3	Suspended beam	320	90	0.5	Gold
4	Biasing pads	100	80	2.3	Gold
5	Meanders				
	(m1)	40	10	0.5	Gold
	(m2)	20	10	0.5	
	(m3)	30	10	0.5	
6	Signal line dielectric	100	100	0.3	Si$_3$N$_4$
7	Anchor × 4	10	5	2.5	Gold

μm micrometres
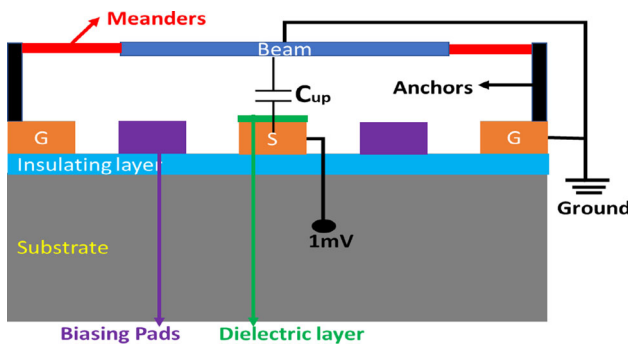
Fig. 6 The schematic view of the proposed switch without actuation
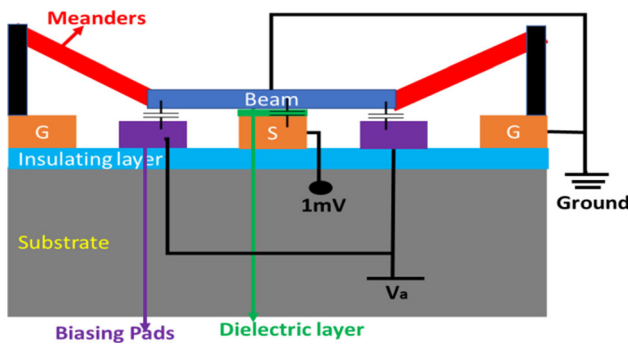
Fig. 7 The schematic view of the proposed switch with actuation

region over the signal line. The dielectric medium made up of silicon nitride is deposited and the remaining portion of photoresist layer is etched to form a dielectric layer of 0.3 μm thickness over the signal line and is shown in Fig. 8i. Again, a photo resist layer is taken as shown in Fig. 8j to define the suspended beam and meanders. A mask is taken to form meanders and suspended beam pattern on the photo resist layer. The defined portion exposed to UV rays is etched and gold metal is deposited in the specified region as shown in the Fig. 8k. The remaining portion of photo resist layer is etched away to form complete design of antenna integrated with RF MEMS switch.

The fabrication issues such as stiction, swelling of released membranes and metal cracking can be overcome by pre-baking and post-baking methods, critical point drying, performing the deposition of thick sacrificial layers to release the membranes and Thermal deposition techniques. The methods improves the high yield of deposited layers and high immune to fabrication tolerances.

4 Results and discussions

4.1 Performance of proposed switch

The proposed structure of the beam consists of central beam and four iterative meanders on either side of beam as shown in Fig. 9. Each meander consists of two iterations such that the first iterative section is of length 60 μm and the second iterative section is of 100 μm. The span length of the second iteration is double that of first iteration i.e., $l_c = 2l_d$ where l_c is of length 40 μm. The iterative meander is used to reduce the spring constant and it is calculated with width $W_c = 10$ μm and thickness as 0.5 μm is

$$K_{iterative\_serpentine} = \frac{4Ew_ct_c^3}{(l_c^3 + l_d^3)} \tag{2}$$

where l_c is the span length of second iteration section of meander, l_d, is the span length of first iteration section of meander, l_e is the length of the connecting meanders and w_c are the width of each block in the meander. The spring constant is the fundamental step to understand the mechanical operation of the switch and is obtained from the Eq. (1) as 0.68 N/m. The pull—in voltage of the fixed–fixed type capacitive shunt switch was expressed as (Guha et al. 2016)

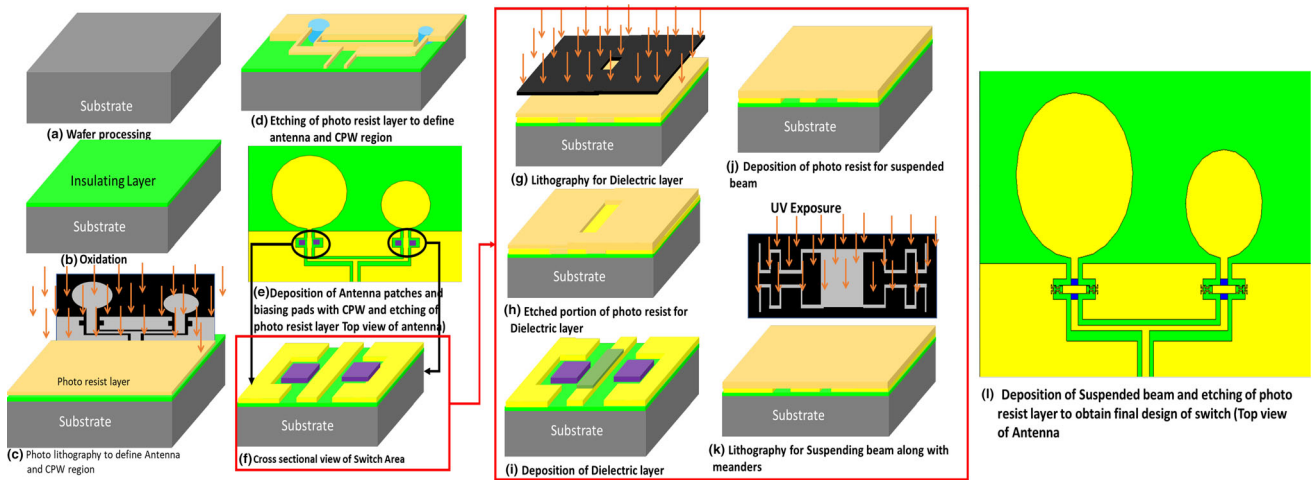$$V_P = \sqrt{\frac{8Kg_0^3}{27\varepsilon_0 A}} \tag{3}$$

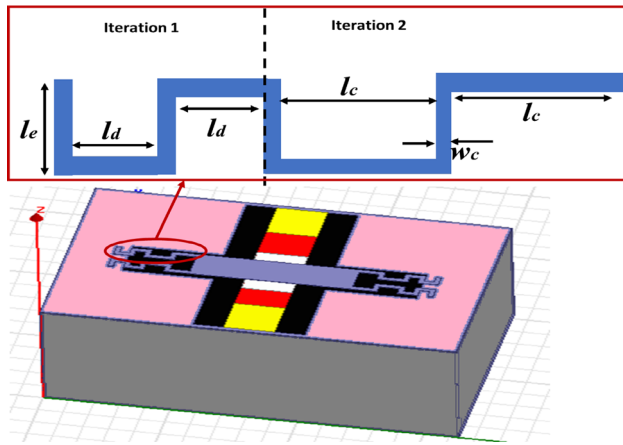**Fig. 8** The fabrication process of the proposed RF MEMS switch using surface micromachining technology

Fig. 9 The schematic view of proposed switch along meanders

Fig. 10 Pull in voltage analysis of switch in COMSOL
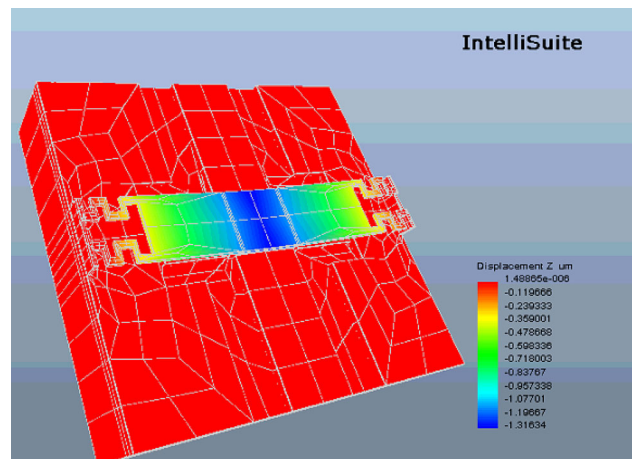
Fig. 11 Pull in voltage analysis of switch in Intellisuite

where K is the spring constant, g_0 is the gap between beam and signal line, A is the overlapping area of the electrodes and ε_0 is the permittivity of the free space. It is observed that the theoretical pull in voltage of the switch obtained from the Eq. (3) is 1.43 V. The proposed switch is designed in COMSOL and Intellisuite tool and are simulated by using electromechanics physics to validate the design.

Figures 10 and 11, illustrates the simulation of proposed switch to displace the beam to its 2/3rd of the gap present between the beam and electrodes. It is observed that the switch displace the 2/3rd gap with actuation voltage of 1.6 V and 1.5 V by using COMSOL and Intellisuite, respectively. Figure 12 describes the calibration of the displacement of beam and it response to the different actuation voltages. It is observed that the beam collapses over the dielectric at 1.6 V which is called as pull in voltage. The simulation carried out using two different tools are closely related to the theoretical values which
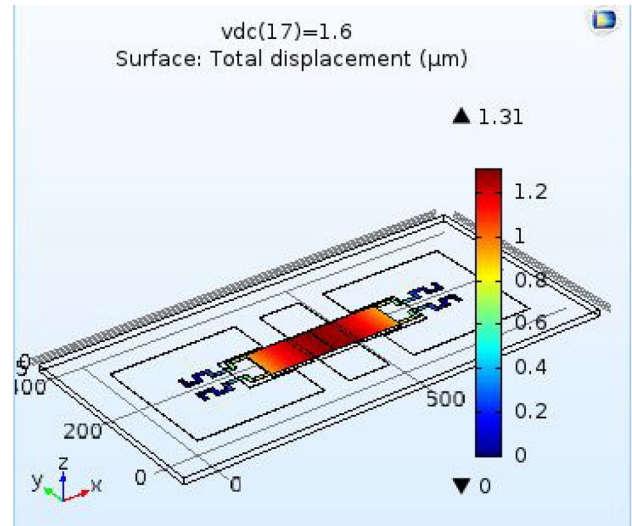
Fig. 12 Displacement calibration of beam at various actuation voltages
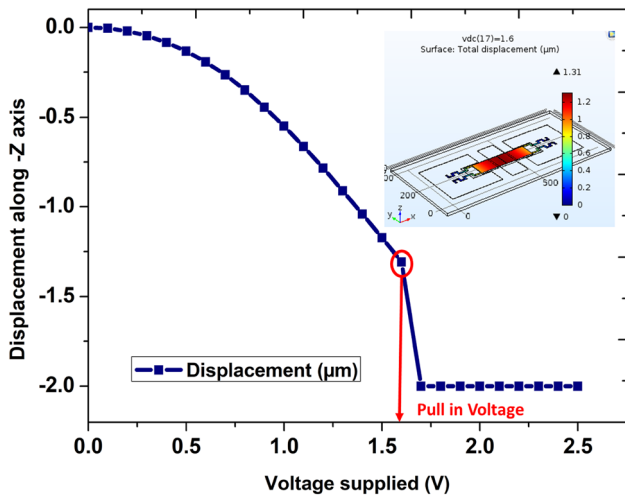
shows the validation of the design. The capacitance developed by the switch at upstate with negligible fringing field capacitance is given by Rao et al. (2018)

$$C_u = \frac{\varepsilon_0 A}{g_0 + \frac{t_d}{\varepsilon_r}} \tag{4}$$

where t_d is the silicon nitride dielectric thickness, ε_r is the dielectric constant of silicon nitride which is present over the signal line, ε_0 is the dielectric constant of free space and A is the actuation area of between the electrodes.

When the voltage is applied between the beam and biasing pads the beam bends towards the biasing pads and the capacitance between them increases. The capacitance at which the beam collapses on the dielectric layer is called down state capacitance and is given as

$$C_{down} = \frac{\varepsilon_0 w_b}{t_d} \left[\varepsilon_r W_s + W_{bp} \right] \tag{5}$$

where w_b is the width of the beam, W_s is the width of the signal line and W_{bp} is width of the biasing pads. The downstate capacitance consists of two components: the capacitance developed by the signal line and biasing pads with the suspended beam. The capacitance across beam and signal line utilizes the silicon nitride as a dielectric medium and capacitance across beam and biasing pads utilizes air as a dielectric medium.

Theoretically the up and down state capacitance obtained from the Eqs. (4) and (5) are 37 fF and 1.99 pF and from the Figs. 13 and 14 the simulation results of the switch at up and downs stated conditions are obtained as 34.5 fF and 1.8 pF, respectively which are approximately equal to the theoretical results. The transition time of the switch from ON state to OFF state is depends on actuation and pull in voltage as well as resonant frequency and is expressed as (Kumar et al. 2018)
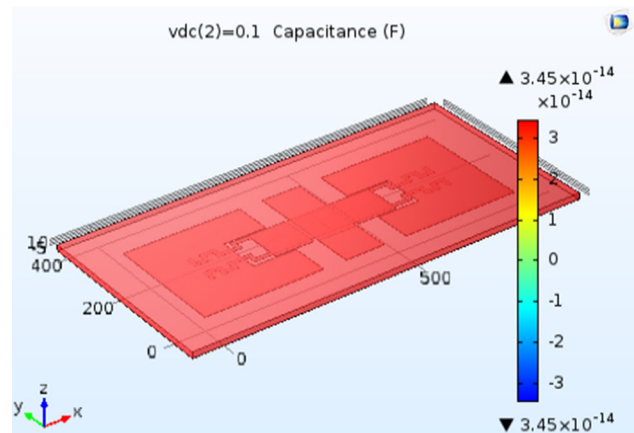

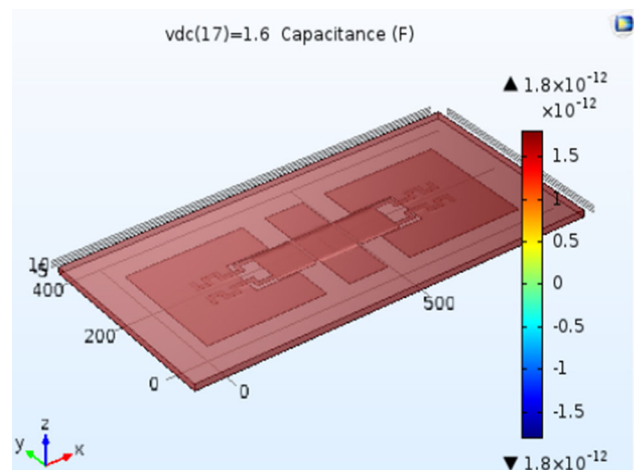**Fig. 13** Simulation of up state capacitance

Fig. 14 Simulation of down state capacitance

$$T_s = \frac{3.67 V_p}{V_s \omega_0}. \tag{6}$$

The switching time from the Eq. (6) is 16 μs which shows low transition time. The performance of the switch is also depending on the S-parameters associated with the switch. To obtain RF performance characteristics the switch is designed and simulated using HFSS 13.0 V tool in wide range of frequencies from 1 to 100 GHz. The switch exhibits return and insertion losses during transmission state i.e., in upstate and produces isolation during OFF state i.e., down state.

The capability of the switch to obtain best switching conditions is analysed by observing the damping factor of the meanders and beam suspended over the signal line. The controllability of the beam to regain its original position (upstate) after the actuation voltage is released achieved by the damping factor which is given by

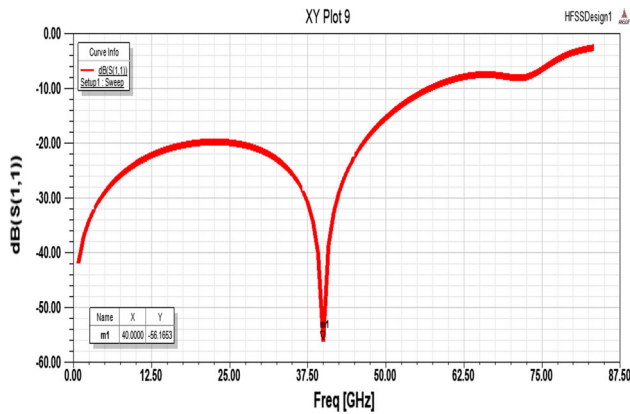$$b_s = \frac{3}{2\pi} \frac{\mu A_{ov}^2}{g_a^3} \tag{7}$$

Fig. 15 Return loss in UP state

Fig. 16 Insertion loss in UP state

where b_s is the damping coefficient of meanders connected with beam, μ is air viscosity which is given as 1.885×10^{-5} Pa and A_{ov} is the total overlapping area during actuation From the Eq. (7) the damping coefficient is obtained as 7.2×10^{-6} Pa/m which very low damping to make the beam settle faster.

The switch shows the return loss of greater than − 56 dB at 40 GHz as a center frequency and can be utilized in the frequency band from 20 to 68 GHz as shown in Fig. 15 and from Fig. 16 shows that the switch exhibits good insertion loss of − 0.19 dB at 41 GHz. Hence a large of amount of signal without much losses is transmitted by the switch and efficiently used for millimeter wave applications up to 68 GHz.

The switch is actuated to turn off and the isolation produced during this state is obtained as − 37.9 dB at 45 GHz and the switch shows better isolation from 25 to 88 GHz and is observed in the Fig. 17.

4.2 Performance of the proposed antenna

4.2.1 Patch antenna with switch—B actuated

The proposed switch is designed over the CPW feed of the two circular patch antennas such that the switch over left side antenna which is radiating at 40 GHz is named as switch—A and the switch over the right-side antenna which is radiating at 60 GHz is named as switch—B. These switches control the radiating patches for desired applications.

Initially, when the two switches are not actuated the antennas will be in receiving mode. When the signal is applied on the common feed of the antennas and it is supplied to the antennas through the power divider. During this, when the switch—B is actuated the signal fed into the left side antenna and the signal is radiated at 40 GHz resonant frequency.
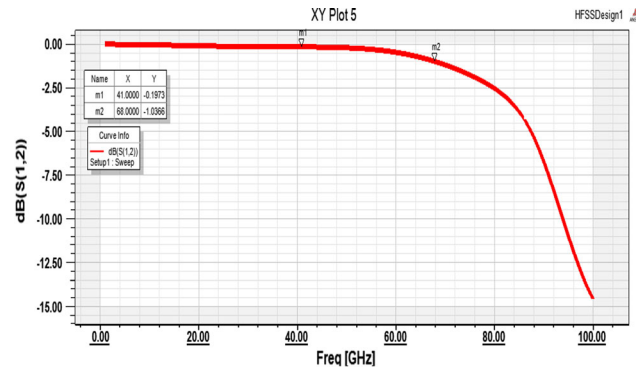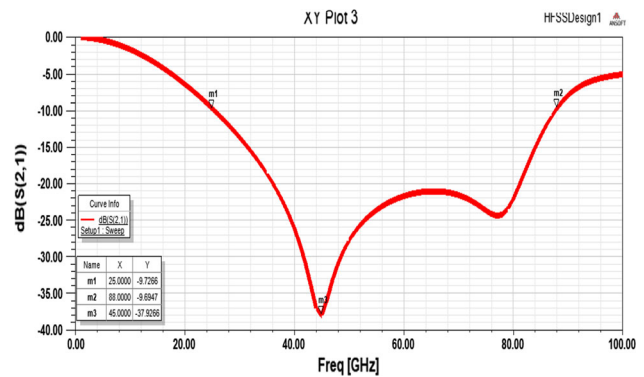

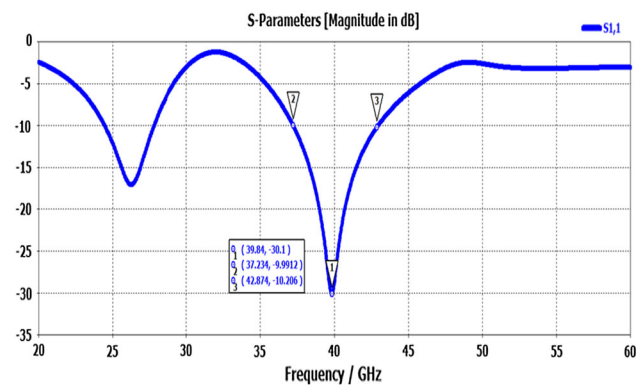**Fig. 17** Isolation of the switch in down state

Fig. 18 Return loss of left side antenna at 40 GHz

The antenna model is designed using CST 15.0 V and from the Figs. 18 and 19, it is observed that the antenna radiates the signal at 39.8 GHz which is approximately close to desired resonant frequency 40 GHz with − 30.1 dB as a return loss and VSWR as 1.2. A high bandwidth of 5.6 GHz is achieved during the transmission of the signal with Left side antenna at 40 GHz.

The proposed antenna is simulated in far field region and the antenna shows directivity of 3.21 dB with radiating efficiency of 0.03 dB and total efficiency of 0.022 dB at
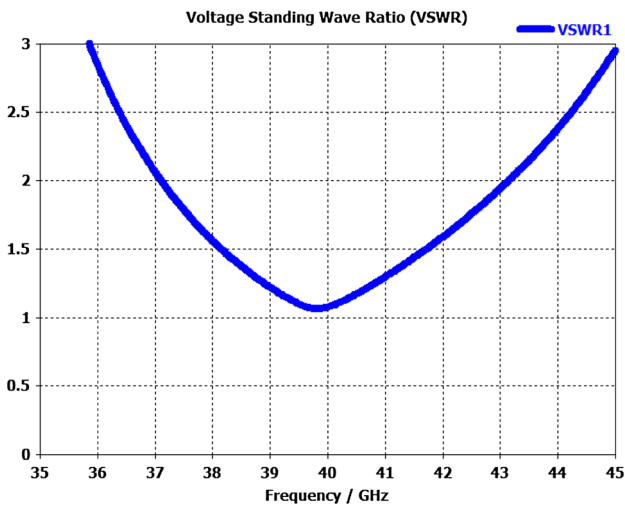
Fig. 19 VSWR characteristics of left side antenna at 40 GHz
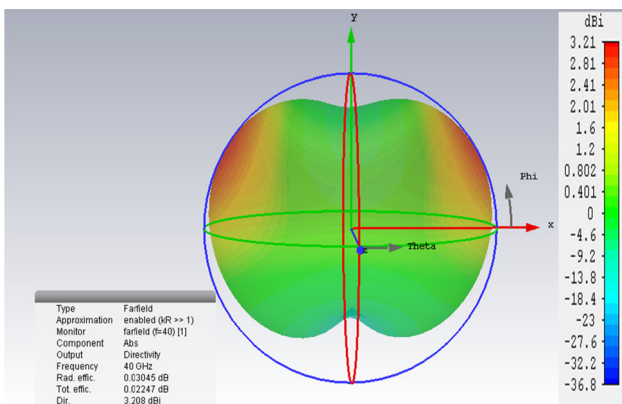

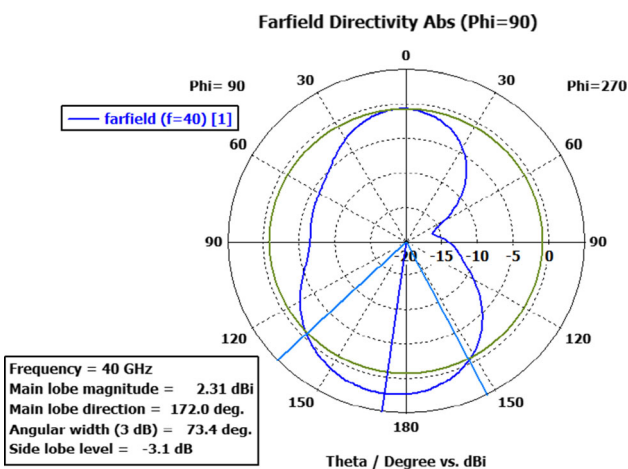Fig. 20 3D far field radiation pattern left side antenna at 40 GHz

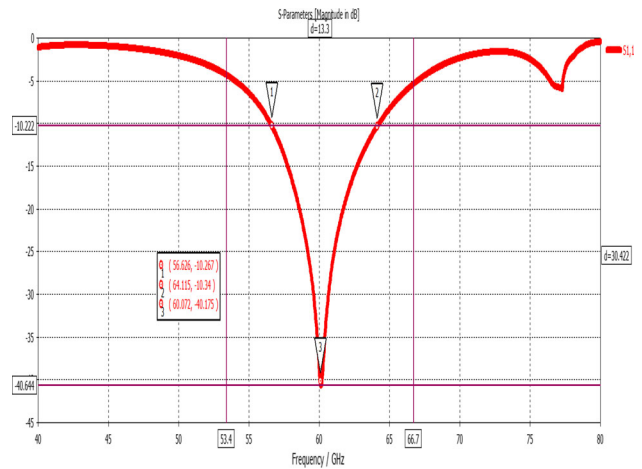Fig. 21 2D far—field radiation of left side antenna at 40 GHz

Fig. 22 Return loss of right-side antenna at 60 GHz

40 GHz has been observed from the Fig. 20. The gain of antenna is 2.31 dB at 172° with a 3 dB angular width of 79.4° is observed from the Fig. 21. The observed characteristics shows the better reliability of the proposed antenna at 40 GHz.

4.2.2 Patch antenna with switch—A actuated

The signal is propagated at 40 GHz unless the frequency band is congested. When the signal traffic is high at 40 GHz band the switch—A is actuated to OFF state and switch—B is in upstate with unactuated such that it allows the signal to radiate at 60 GHz frequency.

The right side antenna is simulated when the switch—B is in up state and it shows the return loss of − 40.1 dB at 60.02 GHz as shown in Fig. 22 with a bandwidth of 7.5 GHz and also Fig. 23 describes contains good VSWR of 1.02 at 59.9 dB.

The right-side antenna is simulated in far field region and the antenna contains the directivity of 5.02 dB at 151° with a 3 dB angular width of 87.6°, the radiating efficiency of 0.021 dB and total efficiency of 0.01 dB is observed from the Figs. 24 and 25. The proposed antenna shows high performance characteristics and can be highly utilized for 5G mobile communication applications which are placed ate the mobile switching center and base transceiver stations.

The proposed switch is compared with the existing novel switch which is presented in Table 2 and analyzed that the novel iterative meanders offers low spring constant such that very less pull in voltage is occurred and the transition time is very less (16 μs). The materials taken for the proposed switch is same as the existing switch but the proposed switch is optimized to work on millimeter wave frequencies by changing the overlapping areas. The
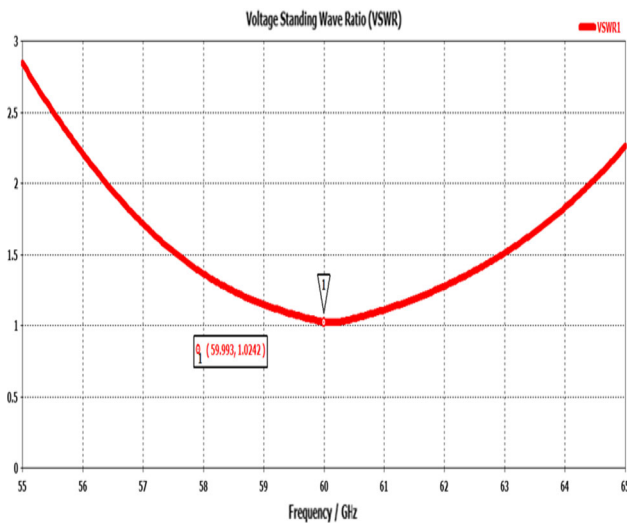
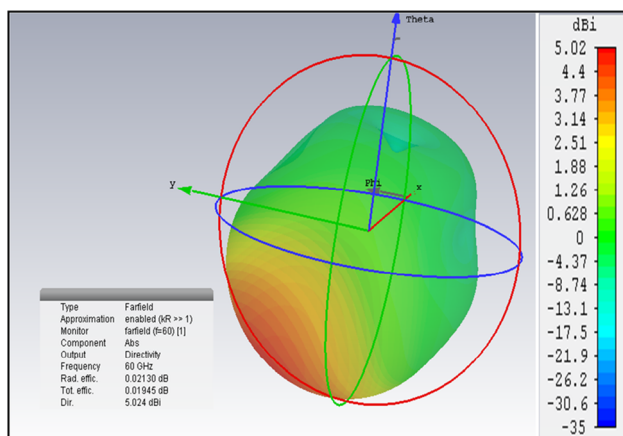**Fig. 23** VSWR characteristics of right side antenna at 60 GHz

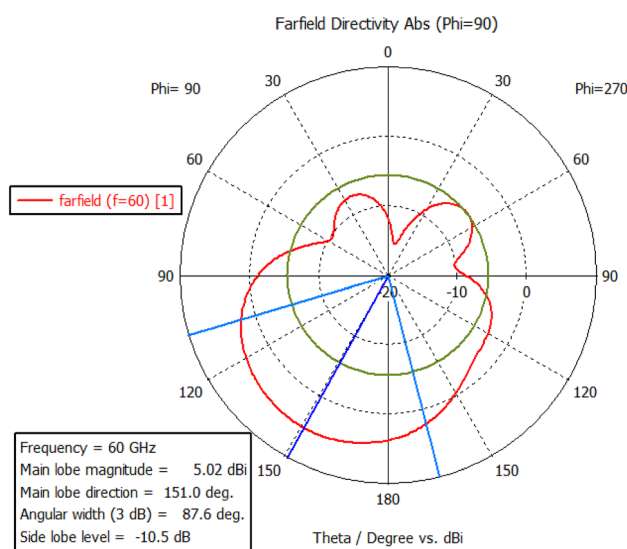**Fig. 24** 3D far field radiation pattern of right side antenna at 60 GHz

Fig. 25 2D far—field radiation of right side antenna at 60 GHz

Table 2 Comparison of the proposed switch with previous work

Parameter/component	Xu et al. (2018)	Proposed switch
Substrate	Silicon	Silicon
Dielectric layer	Silicon nitride	Silicon nitride
Suspended beam material	Gold	Gold
Suspended beam thickness	1 μm	0.5 μm
Pull—in voltage	14 V	1.6 V
Switching time	24.2 μs	16 μs
Cd	–	Theoretical: 1.99 pF
		Simulated: 1.8 pF
Cu	–	Theoretical: 37 fF
		Simulated: 34.5 fF
Insertion loss	< 0.1 dB	< 0.1 dB
Return loss	− 30 dB	− 56 dB
Isolation loss	− 45.3 dB	− 37.9 dB

downstate capacitance is enhanced for large capacitance ratio such that the switch shows better execution of ON and OFF states. The proposed switch shows high very low return losses than existing switch and good isolation at millimeter wave frequencies.

The existing switch is taken on the feeds of two circular patches of antenna of equal sizes connected to rectangular patches. The proposed switch is also taken on the CPW feeds of the circular patches of antenna. The proposed antenna integrated with iterative meander switch results are compared with existing antenna in literature and the comparison is presented in the Table 3. The proposed antenna is made to operate on two frequencies only which serves for 5G mobile communications, hence to achieve this the switches are actuated alternatively.

The proposed antenna is designed to work at only two 5G mobile communication frequencies rather than four frequencies. Initially the mobile station acquires the communication at the frequency of 40 GHz, if the signal congestion occurs the frequency of the communication signal is shifted to 60 GHz which is another frequency band allocated for 5G mobile communications. Whereas the existing switch and antenna is used to reconfigure the frequency with in the frequency band around 16 GHz.

5 Conclusions

This work presents the design and simulation of two circular patch antennas integrated with the novel iterative type RF MEMS switch on a single substrate. The proposed switch is operated at very low pull in voltage of 1.6 V with fast transition time of 1.63 μs. The switch exhibits good isolation of − 37.5 dB and it is efficiently used to block the

Table 3 Comparison of the proposed switch with previous work

Switch combinations	Xu et al. (2018)	Proposed work
Both switches ON state	− 35 dB @ 16.4 GHz	–
Switch A is OFF and switch B is ON	− 32 dB @ 16.5 GHz	− 40.1 dB @ 60.02 GHz
Switch A is ON and switch B is OFF	− 24 dB @ 14.5 GHz	− 30.1 dB @ 39.8 GHz
Both switches OFF	− 42 dB @ 16.7 GHz	–

signal passing to the antennas when they are OFF state. The antennas which are integrated with the switches exhibits high band width of 5.6 GHz and 7.5 GHz at 40 GHz and 60 GHz, respectively. The proposed reconfigurable antenna can be alternatively switched between 40 and 60 GHz by using proposed switches and can be efficiently used in in base transceivers stations and mobile switching center for transmitting and receiving the mobile signals.

References

Anagnostou D, Christodoulou CG, Lyke JC (2001) Smart reconfigurable antennas for satellite applications. In: IEEE Core Technologies for Space Systems Conference, Colorado Springs, CO

Aydemir M, Cengiz K (2016) A potential architecture and next generation technologies for 5G wireless networks. In: Signal processing and communication application conference (SIU), 2016 24th (pp 277–280). IEEE

Borah J, Sheikh TA, Roy S (2016) Compact CPW-fed tri-band antenna with a defected ground structure for GSM, WLAN and WiMAX applications. Radioelectr Commun Syst 59(7):319–324

Brown ER (1998) RF-MEMS switches for reconfigurable integrated circuits. IEEE Trans Microw Theory Tech 46:1868–1880

George R et al (2017) Design of series RF MEMS switches suitable for reconfigurable antenna applications. In: 2017 International conference on circuit, power and computing technologies (ICCPCT) 2017, pp 1–5

Guha K, Kumar M, Parmar A, Baishya S (2016) Performance analysis of RF MEMS capacitive switch with non-uniform meandering technique. Microsyst Technol 22(11):2633–2640

Haraz OM et al (2015) Design of a 28/38 GHz dual-band printed slot antenna for the future 5G mobile communication networks. In: Antennas and propagation and USNC/URSI National Radio Science Meeting, 2015 IEEE international symposium on IEEE, 2015

Hong W, Baek KH, Lee Y, Kim Y, Ko ST (2014) Study and prototyping of practically large-scale mmWave antenna systems for 5G cellular devices. IEEE Commun Mag 52(9):63–69

Katehi LPB, Harvey JF, Brown E (2002) MEMS and Si micromachined circuits for high frequency applications. IEEE Trans Microw Theory Tech 50(3):858–866

Kumar PA, Sravani KG, Sailaja BVS, Vineetha KV, Guha K, Rao KS (2018) Performance analysis of series: shunt configuration based RF MEMS switch for satellite communication applications. Microsyst Technol. https://doi.org/10.1007/s00542-018-3907-1

Mukherjee A, Cheng J-F, Falahati S, Koorapaty H, Kang DH, Karaki R, Larsson D (2016) Licensed-assisted access LTE: coexistence with IEEE 802.11 and the evolution toward 5G. IEEE Commun Mag 54(6):50–57

Niu Y, Li Y, Jin D, Su L, Vasilakos AV (2015) A survey of millimeter wave communications (mmWave) for 5G: opportunities and challenges. Wirel Netw 21(8):2657–2676

Öjefors E (2004) Micromachined antennas for integration with silicon based active devices. Uppsala University, Uppsala

Pourziad A, Nikmehr S, Veladi H (2013) A novel multi-state integrated RF MEMS switch for reconfigurable antennas applications. Prog Electromagn Res 139:389–406. https://doi.org/10.2528/PIER13012303

Rao KS, Kumar PA, Guha K, Sailaja BVS, Vineetha KV, Baishnab KL, Sravani KG (2018) Design and simulation of fixed–fixed flexure type RF MEMS switch for reconfigurable antenna. Microsyst Technol. https://doi.org/10.1007/s00542-018-3983-2

Sharma AK, Gupta N (2012) Material selection of RF-MEMS switch used for reconfigurable antenna using Ashby's methodology. Prog Electromagn Res Lett 31:147–157

Xu Y, Tian Y, Zhang B, Duan J, Yan L (2018) A novel RF MEMS switch on frequency reconfigurable antenna application. Microsyst Technol 24(9):3833–3841. https://doi.org/10.1007/s00542-018-3863-9

Zalud V (2002) Wireless cellular mobile communications. Radioengineering 11(4):1–5

Zhou L, Sharma SK, Kassegne SK (2007) Reconfigurable microstrip rectangular loop antennas using RF MEMS switches. Microw Opt Technol Lett 50(1):252–256. https://doi.org/10.1002/mop.23042